THE SPECIATION OF ARSENIC IN IRON OXIDES IN MINE WASTES FROM THE GIANT GOLD MINE, N.W.T.: APPLICATION OF SYNCHROTRON MICRO-XRD AND MICRO-XANES AT THE GRAIN SCALE

Stephen R. WALKER and Heather E. JAMIESON[§]

Department of Geological Sciences and Geological Engineering, Queen's University, Kingston, Ontario K7L 3N6, Canada

Antonio LANZIROTTI

Consortium for Advanced Radiation Sources, University of Chicago at Brookhaven National Laboratory, Upton, New York 11973, USA

Claudio F. ANDRADE

Department of Geological Sciences and Geological Engineering, Queen's University, Kingston, Ontario K7L 3N6, Canada

Gwendy E.M. HALL

Geological Survey of Canada, 601 Booth Street, Ottawa, Ontario K1A 0E8, Canada

ABSTRACT

Understanding the solid-phase speciation of arsenic in soils and sediments is important in evaluations of the potential mobility of arsenic and of its bio-availability in the environment. This is especially true in mine-influenced environments, where arsenic commonly is present at concentrations two and three orders of magnitude above quality criteria for soils and sediments. Arsenic-bearing particulates dispersed through hydraulic transport or aerosol emissions can represent a persistent source of contamination in sediments and soils adjacent to past mining and metallurgical operations. The stability and mobility of arsenic associated with these phases depend on the chemical form and oxidation state of the arsenic and the interaction with post-depositional geochemical conditions. The Giant mine in Yellowknife, Northwest Territories, roasted arsenic-bearing gold ore from 1949 to 1999. The roasting process decomposed arsenic-bearing sulfides (pyrite and arsenopyrite) to produce a calcine containing fine (generally <50 μm) arsenic-bearing iron oxides. We have applied synchrotron As *K*-edge micro X-ray Absorption Near-Edge Structure (μXANES) and μXRD as part of a grain-by-grain mineralogical approach for the direct determination of the host mineralogy and oxidation state of As in these roaster-derived iron oxides. The grain-scale approach has resolved potential ambiguities that would have existed had only bulk XANES and XRD methods been applied. Using combined optical microscopy, electron microprobe and μXRD, we have determined that the roaster-iron oxides are nanocrystalline grains of maghemite containing <0.5 to 7 wt.% As. Some of these arsenic-bearing nanocrystalline grains are a mixture of maghemite and hematite. All roaster iron oxides, including those present in 50-year-old tailings, contain mixtures of As^{5+} and As^{3+}. The persistence of As^{3+} in roaster-derived maghemite in shallow subareal (oxidized) shoreline tailings for over 50 years suggests that the arsenic is relatively stable under these conditions, even though As^{3+} is a reduced form of arsenic, and maghemite is normally considered a metastable phase.

Keywords: arsenic speciation, maghemite, hematite, micro-XANES, micro-XRD, gold ore, ore roasting, Giant mine, Northwest Territories.

SOMMAIRE

Une connaissance de la spéciation des phases solides contenant l'arsenic dans les sols et les sédiments s'avère importante dans l'évaluation de la mobilité potentielle de l'arsenic et sa biodisponibilité dans l'environnement. Ceci s'applique en particulier aux milieux voisins des exploitations minières, où l'arsenic est présent à des concentrations deux ou trois fois supérieures aux indices de qualité des sols et des sédiments. Les particules porteuses d'arsenic dispersées par transport hydraulique ou aéroportées peuvent représenter une cause persistante de contamination des sédiments et des sols près des installations minières et métallurgiques. La stabilité et la mobilité de l'arsenic associé à ces phases seraient régies par la forme chimique et le

---

§ *E-mail address*: jamieson@geol.queensu.ca

taux d'oxydation de l'arsenic et le rôle des conditions géochimiques suite à la déposition. A la mine Giant, Territoires du Nord-Ouest, le minerai aurifère a été grillé de 1949 à 1999. Le processus de grillage a mené à la décomposition des sulfures porteurs d'arsenic (pyrite et arsénopyrite) pour produire un calcinat contenant des oxydes de fer arsenifères à granulométrie fine (<50 μm). Nous nous sommes servis de la micro-absorption des rayons X près du seuil K (rayonnement synchrotron; μXANES) et de la microdiffraction X pour effectuer une étude minéralogique grain par grain afin de déterminer la minéralogie de l'hôte et le taux d'oxydation de l'arsenic dans ces oxydes de fer produits au cours du grillage. Cette approche détaillée nous a permis de résoudre les ambiguïtés potentielles si seules les méthodes XANES et diffraction X appliquées aux échantillons globaux étaient disponibles. En utilisant une combinaison de microscopie optique, microsonde électronique et microdiffraction, nous avons déterminé que les oxydes de fer issus du grillage contiennent des grains nanocristallins de maghémite avec entre <0.5 et 7% d'arsenic (poids). Dans certains cas, les grains arsenifères nanocristallins sont un mélange de maghémite et d'hématite. Tous les oxydes de fer issus du grillage, y inclus ceux qui constituent les rejets miniers vieux de cinquante ans, contiennent un mélange de As^{5+} et As^{3+}. D'après la persistance de l'As^{3+} dans la maghémite issue du grillage dans les rejets oxydés le long de la rive et exposés à l'atmosphère depuis cinquante ans, l'arsenic serait relativement stable sous ces conditions, malgré la forme réduite de l'arsenic et la métastabilité acceptée de la maghémite.

(Traduit par la Rédaction)

Mots-clés: spéciation de l'arsenic, maghémite, hématite, micro-XANES, microdiffraction X, minerai d'or, grillage du minerai, mine Giant, Territoires du Nord-Ouest.

INTRODUCTION

The mobility and toxicity of arsenic depend on its speciation (chemical form and oxidation state). In the dissolved phase, arsenic is most often present as arsenate ($H_2AsO_4^-$ or $HAsO_4^{2-}$) or arsenite ($H_3AsO_3^0$), with arsenate being the more oxidized and thermodynamically stable form at ambient conditions. However, disequilibrium of arsenic species is well documented (Inskeep *et al*. 2002, Smedley & Kinniburgh 2002), and both reduced and oxidized forms commonly occur together. This fact is important, as arsenite is generally regarded as the more mobile (Masscheleyn *et al*. 1991) and more toxic in the environment (Naqvi *et al*. 1994, Winship 1984).

The concentrations of specific dissolved species present in porewater and groundwater are a measure of arsenic mobility. However, the solid components of the sediments, soils and mine waste are the ones that provide the geochemical or biogeochemical substrate that controls arsenic partitioning to the aqueous phase. In addition, mining and metallurgical processing (including smelting and roasting of ores) produce fine particulate arsenic-bearing solid phases that can be transported and deposited in the local and regional environment by aerial and hydraulic processes (Bérubé *et al*. 1973, Ragaini *et al*. 1977, Hocking *et al*. 1978, Mok & Wai 1990, Moore & Luoma 1990, Henderson *et al*. 1998, Reimann *et al*. 2000). It is important to understand the solid-phase speciation of arsenic in mining and metallurgical products, as it may differ from the background speciation, or from solid phases produced by post-depositional adsorption or precipitation reactions. The multiple origins of arsenic-bearing phases in soils and sediments adjacent to mining and metallurgical operations suggest that a grain scale micro-analytical approach may be particularly well suited for determining arsenic speciation in these complex materials.

In the present study, we establish a method to investigate the solid-phase speciation of arsenic in silt-sized soil, sediment and tailings particles. We have combined powder XRD and bulk XANES with optical microscopy and grain-by-grain micro-analysis using EPMA, and synchrotron μXRD and μXANES. We highlight findings of complex speciation of arsenic in roaster-derived iron oxide phases from the Giant mine, Yellowknife, Northwest Territories, and show the utility of applying synchrotron-based micro-analytical techniques at the grain scale (20 to 50 μm). Grain-scale analyses clarify potential ambiguities that would otherwise exist in these materials based on bulk analyses and petrography alone.

BACKGROUND INFORMATION

In studying areas influenced by mining and metallurgical processing, it is important to distinguish between primary and secondary phases (Jambor 1994, Jambor & Blowes 1998, Manceau *et al*. 2002). Primary phases are those that originate from the milling process (both unreacted and reacted minerals and metallurgical products), and secondary minerals are those formed by reactions following deposition in the environment (*e.g*., weathering or precipitation). Metallurgical products are designated as primary anthropogenic phases in order to distinguish between anthropogenic influences (metallurgical chemical reactions in the mill) and natural geochemical processes (Manceau *et al*. 2002). Observing physical or chemical changes to primary arsenic-bearing phases in the environment may provide evidence of the long-term stability or behavior of arsenic in the environment. Secondary arsenic-bearing minerals or arsenic sorbed to other primary or secondary minerals is direct evidence of the attenuation of arsenic in soils, sediments and mine waste (*i.e*., sequestering

by solid-phase transformation, or removal from the aqueous phase by sorption or precipitation).

For a typical gold-roasting operation, the primary phases would therefore include ore minerals (*e.g.*, arsenopyrite and pyrite), and gangue minerals (*e.g.*, quartz, other silicates and carbonates) and anthropogenic solid products of reaction produced during milling [*e.g.*, hematite (α-Fe_2O_3) and maghemite (γ-Fe_2O_3) derived from the thermal oxidation of pyrite and arsenopyrite].

Solid-phase speciation of arsenic in geochemical cycling, fate and bio-availability

Bonding in arsenic-bearing minerals is dominantly ionic where coordinated with oxygen and covalent where coordinated with sulfur, iron or itself (Greenwood & Earnshaw 1998). Arsenic in both ionic and covalent solids can exhibit a wide range in oxidation number: +5 for arsenates (*e.g.*, scorodite, $FeAsO_4\bullet2H_2O$) and +3 for arsenites (*e.g.*, arsenolite, As_2O_3 and schneiderhöhnite, $Fe^{2+}Fe^{3+}_3As^{3+}_5O_{13}$), +3 for orpiment ($As_2S_3$), +2 for realgar ($As_4S_4$), 0 for elemental arsenic (As), –1 for arsenopyrite, and –2 for westerveldite (FeAs). Arsenic of different oxidation-states can also be incorporated in solid solution in mineral phases. For example, As^{1-} substitutes for S in pyrite (*e.g.*, Simon *et al*. 1999, Savage *et al*. 2000), and AsO_4 substitutes for SO_4 in jarosite [$KFe_3(SO_4)_2(OH)_6$: Dutrizac & Jambor 2000, Savage *et al*. 2000, Paktunc & Dutrizac 2003, Savage *et al*. 2005)]. Arsenate and, in some cases, arsenite, can also sorb strongly onto clay minerals and oxyhydroxides of iron, aluminum and manganese (Smedley & Kinniburgh 2002, Hering & Kneebone 2002, and references therein). Bostick & Fendorf (2003) have shown that under aqueous reducing conditions, arsenite can be reduced to form an arsenopyrite-like precipitate on the surface of iron sulfides.

Whether sorbed or structurally bound, understanding the kinetics and mechanisms of release of As in the context of equilibrium relationships involving solids and solution is necessary to evaluate short- and long-term mobility and bio-availability (Huang & Fujii 1996, Hering & Kneebone 2002). For example, high-surface-area arsenic-bearing iron oxyhydroxides, which are amorphous or poorly crystalline, may recrystallize to more stable phases and desorb arsenic (Fuller *et al*. 1993, Waychunas *et al*. 1993, Smedley & Kinniburgh 2002, Paktunc *et al*. 2004). However, such processes may be slow in nature owing to the presence of strongly surface-sorbed or coprecipitated ions, including arsenate (Cornell & Schwertmann 1996). Also, redox conditions can profoundly affect partitioning of arsenic between aqueous and solid species (*e.g.*, Hering & Kneebone 2002, Smedley & Kinniburgh 2002, Cummings *et al*. 1999, Nickson *et al*. 2000, Harvey *et al*. 2002), an important consideration in natural environments, where biogeochemical conditions are rarely static.

With respect to bio-availability of arsenic that has been orally ingested by humans, it is clear from existing work that solid-phase arsenic is less bio-available than arsenic in solution (Ruby *et al*. 1999, Valberg *et al*. 1997). However, in the solid state, the amount that is bio-available depends on a number of factors, including oxidation state, mineralogy, grain size, surface area and morphological properties, such as encapsulation or rinding of grains (Ruby *et al*. 1999, Bhumbla & Keefer 1994).

Anthropogenic iron–arsenic oxides

Anthropogenic arsenic-bearing iron oxides have been identified in the environment (soils, sediments, tailings and house dust) adjacent to sulfide smelting and roasting operations (*e.g.*, Davis *et al*. 1996, McCreadie *et al*. 2000). Roasting of pyrite and arsenopyrite produces iron oxides with a concentric distribution or porous "spongy" texture depending on the pathway (formed by way of a pyrrhotite intermediate phase or not) and temperature of formation (Carter & Samis 1950, Jorgensen & Moyle 1981, Arriagada & Osseo-Asare 1984, Robinson 1988, Grimsey & Aylmore 1992, Dunn *et al*. 1995). However, there is limited understanding of the solid-phase speciation of arsenic in iron oxides derived from roasting. The presence of an unidentified non-sulfide arsenic-bearing phase or phases has been inferred on the basis of a sizeable excess of arsenic to sulfur in some calcines (*e.g.*, Arriagada & Osseo-Asare 1984). Roaster-derived iron oxides are an example of primary anthropogenic arsenic-bearing solids that have a high arsenic content (several weight percent) and have little analogy to better-studied naturally occurring primary minerals such as arsenopyrite, and secondary minerals such as arsenic-bearing iron oxyhydroxides and arsenic sulfides.

For many low-temperature geochemical systems, formation of iron oxides and oxyhydroxides as amorphous or crystalline nanoparticles (*i.e.*, 1 to 100 nm in diameter, Waychunas 2001) is expected over short to medium time-scales (Banfield & Zhang 2001, Waychunas 2001, Hochella 2002). Furthermore, industrial methods of iron oxide production at elevated temperatures also produce nanocrystalline iron oxides (*e.g.*, Morjan *et al*. 2003, Deb *et al*. 2001). In recent experiments, Eneroth & Koch (2003) determined that thermal oxidation of iron sulfides (pyrite and marcasite) can result in small sizes (15 to 60 nm) of the average crystallite in the resulting iron oxides. If roaster- or smelter-derived phases (grains) are nanoparticle composites, they may exhibit modified phase-stability relationships and different reaction-kinetics in comparison to their microscopic and macroscopic counterparts (Banfield & Zhang 2001, Navrotsky 2001).

Roasting of gold ore at the Giant mine

Mineralization at the Giant mine, Yellowknife, Northwest Territories, occurs within shear zones as disseminated sulfides in broad silicified zones or quartz–carbonate veins bounded by muscovite or chlorite schist (Boyle 1960, Ellis & Hearn 1990). The gold at the Giant mine is refractory, being mostly incorporated submicroscopically within arsenopyrite, making it unavailable to conventional cyanide extraction. To access this "invisible" gold, ore milling at Giant mine included grinding, flotation, roasting of the flotation concentrate followed by cyanidation (More & Pawson 1978). The roasting of gold ore is a thermal oxidation process that decomposes sulfide minerals such as pyrite and arsenopyrite into porous iron oxides including hematite, maghemite or magnetite, to make the ore amenable to cyanidation (Gossman 1987, McCreadie *et al.* 2000). Roasting at the Giant mine commenced in January 1949 (Grogan 1953) and continued until the mill closed in late 1999.

Roasting at the Giant mine has produced a number of arsenic-bearing wastes, including arsenic trioxide baghouse dust, electrostatic precipitator dust, and calcine residue tailings (cyanidized roasted sulfide concentrate). Baghouse dust has been stored in underground stopes and chambers since 1952 and is the subject of critical evaluation for remediation at the present time (SRK 2002). It has been estimated that some 7900 tonnes of arsenic were released to the environment by stack emissions between 1949 and 1952, since roaster off-gases were not treated at that time [unpublished Environment Canada report referenced by Hocking *et al.* (1978)]. With the exception of the arsenic trioxide dust, roaster-derived wastes have generally been discharged with flotation tailings along with mine and mill water. On a dry tonnage basis, the calcine residue tailings constitute only some 10% of the total tailings discharged, but approximately 70% of the total arsenic by weight (Walker & Jamieson 2002).

ANALYTICAL APPROACH

X-ray absorption spectroscopy (XAS) is effective at determining both oxidation state by X-ray absorption near-edge structure (XANES) and coordination state by extended X-ray absorption fine structure (EXAFS). The XANES approach is capable of determining oxidation states of arsenic by resolving small shifts in the energy position of the As *K* absorption edge (Fendorf & Sparks 1996). The ability to detect As^{3+}-bearing phases may be particularly important since they are generally linked to lower stability and higher toxicity.

Methods of characterization of solids routinely combine results of grain-scale analyses such as optical microscopy, scanning electron microscopy (SEM) and electron-probe micro-analysis (EPMA) with results of bulk analyses such as X-ray diffraction (XRD). Bulk XAS methods have also been successfully applied to the characterization of arsenic-bearing phases in soils (*e.g.*, Morin *et al.* 2002) and mine-waste materials (*e.g.*, Paktunc *et al.* 2003, Morin *et al.* 2003, Savage *et al.* 2000, Foster *et al.* 1998). Comparatively fewer authors (*e.g.*, Strawn *et al.* 2002, Paktunc *et al.* 2004) have utilized micro-XAS methods in arsenic-focused studies. A comprehensive discussion of methods of solid-phase speciation for metals and metalloids, including application of synchrotron micro-XAS methods, can be found in Manceau *et al.* (2002).

EXPERIMENTAL

Samples

Materials selected for this study include: cyanide-treated roaster calcine residue (hereafter referred to as calcine), and a calcine-rich horizon from tailings deposited on the shore of Great Slave Lake about 1950 (hereafter shoreline tailings). The selected tailings-hosted horizon is a subsample of a core collected as part of a larger suite of mine-tailings samples obtained at the site in July 1999. Coring was accomplished by hand-driving aluminum tubes (wall thickness 1.6 mm) with a drop hammer assembly. The tubes were extracted, immediately cut top and bottom to remove any open air-space, sealed and placed in coolers with ice packs. Staff at the Giant mine provided mill samples as slurries in one-liter sealed containers. All samples were frozen shortly after collection (to preserve solid phases from further reaction) and shipped in coolers to laboratory facilities, where they were kept frozen until preparation for analysis.

In order to prepare thin sections, samples were thawed and air-dried at room temperature. Polished thin sections were prepared as intact specimens (plugs extracted from tailings core to preserve stratigraphic relationships) and grain mounts (mill products) using arsenic-free silica glass slides and room-temperature-set epoxy (Sealtronic 21AC–7V by Industrial Formulators), and without the use of added heat or water. Oil was used for all grinding and polishing. Sections were polished to a final thickness of approximately 30 to 40 μm. The final thickness of sections was determined to within 5 μm by measuring edges of polished sections with a micrometer. The slightly thicker sections (standard sections are usually 20 to 30 μm) were necessary to minimize stripping of the fine-grained sections from the slide during final grinding. For some samples, a second "detachable" thin section was made from the same off-cut to facilitate transmission-mode μXRD, which requires removal of the glass slide substrate from beneath the thin section. The preparation of these thin sections was the same as for the other sections, except for the following modifications. Each section was polished and fixed to a prefrosted glass slide using Krazy® glue instead of epoxy. Grinding and polishing

were completed in the same manner as the regular sections, except that the final polished thickness was up to 50 μm. This thickness ensured a robust specimen when the glass slide was removed. Following petrographic examination and target location (see below), the thin section was immersed in an acetone bath (ACS grade) until complete separation of sample from the slide. Detachment time seems to depend on sample grain-size and ranges from 20 minutes for coarser-grained sections to several hours for finer-grained sections. The detached sample was allowed to dry, oriented and carefully pressed on Kapton® tape and placed into a 35-mm cardboard slide-holder for analysis. Kapton® mounted sections were later fixed back onto glass slides using double-sided tape for characterization by EPMA.

Thin sections were inspected and photographed under transmitted and reflected light to identify potential arsenic-bearing phases and to map out targets for micro-beam analysis. Target locations were catalogued using coordinates from a scanned image of the thin section and microscope photographs at multiple scales (Fig. 1) to ensure that the small grains (generally <50 μm

diameter) could be relocated for subsequent analyses on several different micro-beam instruments.

Analyses using μXANES and μXRD

Synchrotron analysis was conducted with the hard X-ray microprobe, X26A, at the National Synchrotron Light Source (NSLS), Brookhaven National Laboratory. A 350-μm collimated monochromatic beam is focused to approximately 10 μm in diameter using a system of Rh-coated Kirkpatrick–Baez mirrors (Eng *et al*. 1995). A monochromatic beam is achieved using a Si(111) channel-cut monochromator. Instrumental resolution is approximately 3.5 eV with reproducibility of the edge position of better than 1 eV. All the μXANES experiments were made by scanning through the As *K* edge (11,867 eV) in fluorescence mode with a Si(Li) detector. MicroXRD experiments are imaged in 2D in transmission mode using a Bruker SMART 1500 CCD diffractometer with a fiber optic taper, in high-resolution mode at 1024×1024 pixels.

Thin sections and standards are placed in cardboard slide-holders and fixed by thumb-screws into the
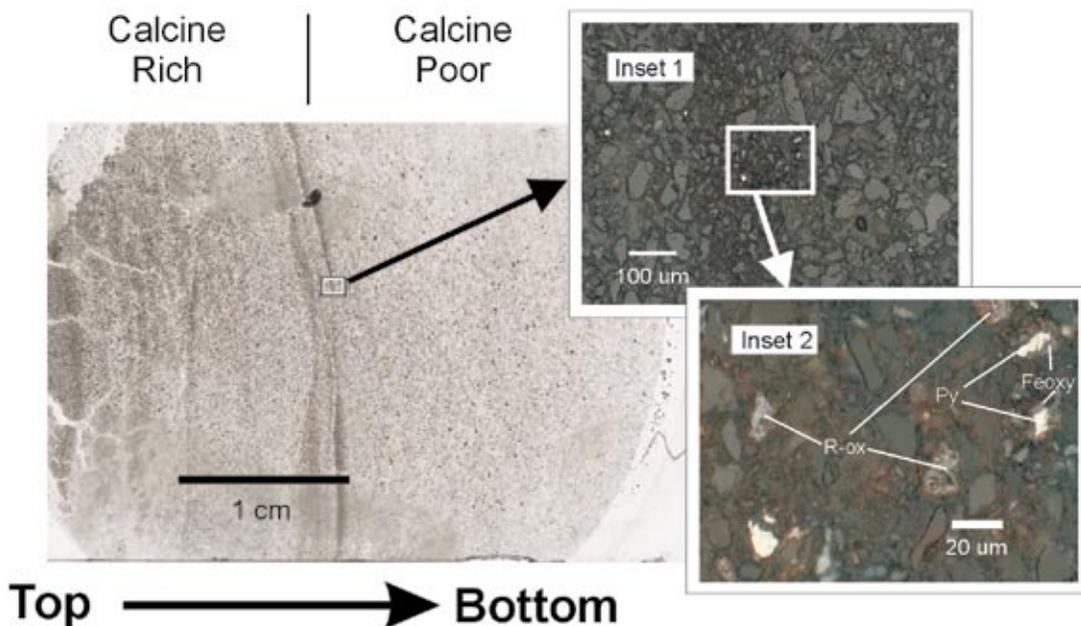

FIG. 1. High-resolution scan of thin section of 50-year-old stratified shoreline tailings subsampled from core taken adjacent to Yellowknife Bay. Insets 1 and 2 are plane-polarized reflected-light photomicrographs that provide progressive magnification of one of the darker silty layers. Darker layers are calcine-rich and contain arsenic-bearing roaster iron oxides (R-ox, Inset 2). Two grains of weathered pyrite (Py) with arsenic-bearing iron oxyhydroxide rims (Feoxy) are identified for comparison. Targets and reference points are recorded as coordinates in mm from scans of the thin sections. Maintaining a consistent orientation allows target spots to be readily located on any microbeam instrument with an X,Y coordinate stage. Photos at multiple scales provide backup for relocating grains.

vertical plastic sample-holder oriented at 45° to the beam in the horizontal plane. This geometry results in an elliptical footprint of the beam on the sample (10 μm in the vertical × 15 μm in the horizontal). Beam penetration through the sample is approximately cylindrical. The small grains being analyzed in these materials (<50 μm) can result in spatial inhomogeneity under the beam, especially since grain depth in the sections can be less than the full thickness of the section (30 to 50 μm). This potential inhomogeneity is handled by observing the sections in transmitted as well as reflected light and by comparing μX-ray fluorescence maps (Fe and As) to scaled photos of thin sections. Two or three analyses can then be conducted through the core and rim of grains

or in regions selected to either investigate or avoid unidentified material buried in the section.

XANES analyses were conducted by scanning across the absorption edge region (11,830 to 11,970 eV) in three segments with a 2- to 4-second dwell time by increment. The step increment was 5 eV in the pre-edge region (11,830 to 11,850 eV), 0.4 eV across the edge (11,850 to 11,890 eV) and 2 eV in the post-edge region (11,890 to 11,970 eV). Primary standards were routinely run, to correct for any shifts in edge position that might occur over time (total range less than 1.5 eV). Each spectrum was normalized to an incident beam flux measured by an upstream ion-chamber, pre-edge background corrected at 11,840 eV, and then normalized to the edge-step (intensity at 11,960 eV). Normalization was done at approximately 100 eV above the absorption edge owing to the significant post-edge oscillations that vary significantly among the various As standards. Standard materials (Table 1, Fig. 2) were selected to cover a wide range of oxidation states exhibited by arsenic (–1 to +5). Primary standards included arsenopyrite, reagent-grade arsenic trioxide, and scorodite. Secondary standards included sodium arsenate, sodium arsenite, schneiderhöhnite, orpiment, realgar and elemental arsenic. Standards were prepared by fine grinding with

TABLE 1. STANDARDS FOR μXANES ANALYSIS

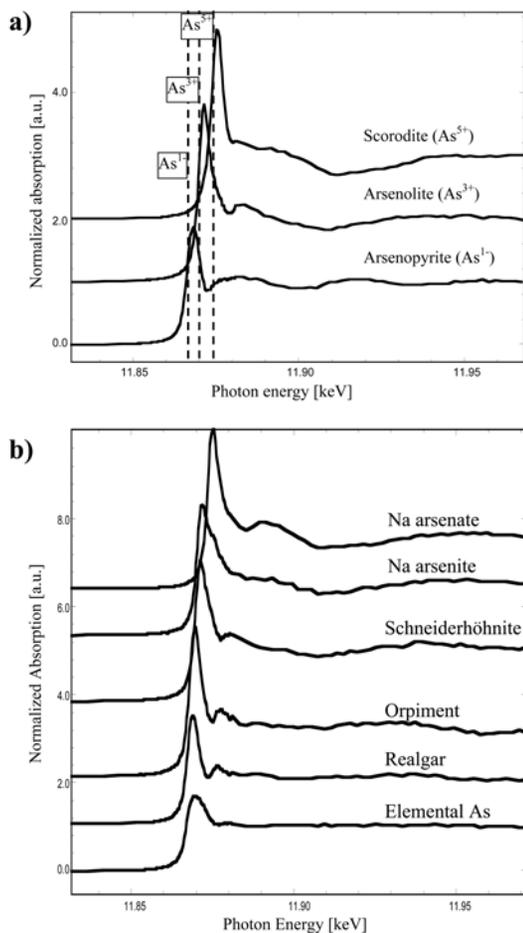|	End-member formula	Source	Edge position†	Norm. peak int.
Primary standards				
Scorodite	FeAs^{5+}O$_4$•2H$_2$O	Laurium, Greece [M6303]	11,873.9*	3.2
Arsenolite	As$^{3-}_2$O$_3$	J.T. Baker reagent	11,870.0*	2.9
Arsenopyrite	FeAsS	Mina La Bufa, Mexico [M5579]	11,867.0	2.2
Secondary Standards				
Sodium arsenate	Na$_2$HAs^{5+}O$_4$•7H$_2$O	J.T. Baker reagent	11,873.5	3
Sodium arsenite	NaAs^{3+}O$_2$•4H$_2$O	J.T. Baker reagent	11,870.2	2.6
Schneiderhöhnite	Fe^{2+}Fe$^{3+}_3$As$^{3+}_5$O$_{13}$	Urucum, Minas Gerais, Brazil	11,869.8	2.7
Orpiment	As$_2$S$_3$	Moldava, Banat, Hungary [M7719]	11,868.2	3.5
Realgar	As$_4$S$_4$	Hunan realgar mine, Shimen, Hunan Province, China [M9900]	11,867.7	2.7
Elemental arsenic	As	Sampson mine, Andreasberg, Harz Mountains, Lower Saxony, Germany [M72]	11,867.0	1.7

FIG. 2. Micro-XANES spectra of standards. a) Primary standards. Vertical dashed lines indicate edge position at first derivative maximum for arsenopyrite (left), arsenolite (middle), and scorodite (right). b) Secondary standards. All spectra are spread vertically for purposes of presentation only.

[Mxxxx]: Miller Museum reference, Department of Geology and Geological Engineering, Queen's University.
† Edge position in eV at first-derivative maximum relative to arsenopyrite, set at 11,867.0 eV. In the case of secondary standards, the edge positions are based on one or two analyses relative to the arsenopyrite standard.
* Estimated error, based on multiple repeat-analyses relative to arsenopyrite, is better than ±0.4 eV.
Norm. peak int.: Normalized peak intensity.

an agate mortar and pestle and HPLC-grade ethanol. To manage self-absorption effects, only the suspended (finest) fraction was retained and mixed with boron nitride (99.9%, <1 μm) to obtain a total concentration of arsenic of approximately 4% (w/w). As arsenic trioxide is slightly soluble in ethanol, an additional dry ground standard of this material was prepared, but there was little difference in the resulting XANES scans. Realgar is known to undergo light-induced transformations to a number of other As_4S_4 polymorphs (Bonazzi *et al*. 1996). To minimize the potential for such reactions, the realgar was stored in the dark immediately following preparation and until analysis. However, no attempt was made to track possible transformations. Each mixture of standard and boron nitride was dispersed as a thin layer onto Kapton tape for analysis.

For μXRD, the incident X-ray beam was tuned to 11,950 eV (1.0375 Å). The distance between the camera and the thin section was fixed at approximately 17 cm, which yielded a calibrated range of *d* values between 2 and approximately 10 Å. Detector calibration was made using SRM 674a diffraction standard α-Al_2O_3. Calibrations and corrections for detector distortions (camera–sample distance, camera tilt and rotation, and the beam center on the camera plane) were done using Fit2D™ software (Hammersley 1998). The two-dimensional patterns were manually inspected to identify the types of reflections present (rings or points). The *d* values of unknowns were determined by integration of the two-dimensional pattern to produce a simulated powder-diffraction pattern. Resolution is about 0.2° 2θ, as measured by integrated peak-widths (FWHM) for the α-Al_2O_3 standard. Unknown phases were identified by comparison with reference powder-diffraction patterns (ICDD 2003).

The experimental conditions in this case utilize monochromatic X-rays without randomization of grain orientation under the beam. Under these conditions, well-defined Debye–Scherrer rings are only obtained where the average size of mineral crystallites is small relative to the diameter of the incident beam and where their orientation is sufficiently random (He 2003, Manceau 2002). Where this is not the case, crystals at diffracting conditions show portions of reciprocal lattice nets, *i.e*., individual spots, arcs or spotty rings, representing discrete diffracted beams.

Bulk X-ray diffraction and bulk XANES

Duplicate samples of the mill calcine (subsample of cone-and-quarter split of M2M) and shoreline tailings (representative sample taken perpendicular to bedding in the same interval as CB1bS3) were submitted for bulk X-ray-diffraction analysis. Analysis utilized a Philips X'Pert MPD fitted with a Co tube operated at 45 kV and 40 mA, with 0.2 rad soller slits, a 20-mm sample mask, ½° divergence slit, *K*β filter and X'Pert

detector. Samples were mounted dry on glass discs rotated at ½ revolution per second with a scan rate of 20 seconds per step, from 5 to 90° 2θ. The material of stratified shoreline tailings was sampled and analyzed in two parts. The first represented the upper, more calcine-rich portion, and the second, the less strongly stratified, lower calcine-content portion (Fig. 1).

Bulk XANES analysis was completed with the mill calcine mounted as a thin powder on Kapton tape using similar analytical conditions as those for μXANES described above, but using an unfocused beam approximately 0.12 mm^2 (0.35 × 0.35 mm). Three random locations were analyzed (single scan each) and averaged after confirming similar spectral shapes for each domain.

Linear-combination fitting of XANES data and PCA analysis

The shape of both bulk and μXANES spectra suggested the presence of multiple oxidation states within the target roaster iron oxide grains (Fig. 3). We found, however, that linear-combination fits with certain standards of different oxidation states (model compounds) gave reasonable fits for the unknown spectra. Linear-combination fitting was made using WinXAS™ v. 2.3, and procedures modified from those described in Ressler *et al*. (2000). Fits may not yield quantitative concentrations since the actual species of arsenic have yet to be determined. However, the proportions calculated on the basis of a consistent set of standards are useful to highlight variability both within and between grains, and between samples. Reported percentages of each model compound in fits are absorption-corrected amounts (normalized to 100%), as calculated with WinXAS. Totals before correction were in the range of 95 to 105%, and generally greater than 98% and lower than 102%. Fitted model spectra at 5% or less gave little noticeable improvements to fits. Analysis of control mixtures of model compounds in macroscopic XAS studies have shown the precision of similar procedures of fitting to be approximately 10% (*e.g*., Foster *et al*. 1998).

To increase objectivity in the linear-combination procedure of fitting, a principal component analysis (PCA) was conducted using routines in the WinXAS™ software in a manner similar to that described in Ressler *et al*. (2000). A total of 14 spectra from M2M were selected for PCA analysis to cover the range of spectral shapes encountered (Fig. 3). All spectra were normalized, calibrated and sectioned to include only the immediate edge-region (11,850 to 11,900 eV). Results of the PCA analysis indicate that at least three components are necessary to fit the data. The first two components accounted for 82% of the fit, and three components accounted for 85%. Transform fits were then applied to the standard spectra (Ressler *et al*. 2000),
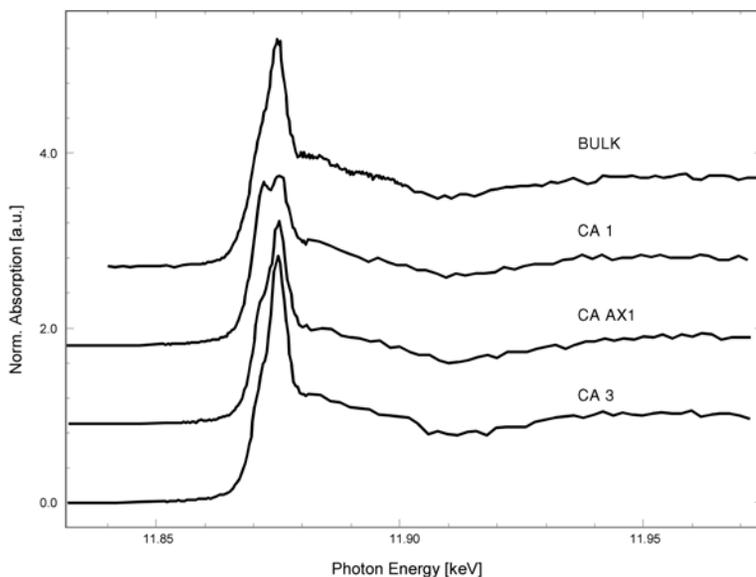
and a quality of fit determined by visual inspection and the residual values calculated by the WinXAS™ software (Table 2).

Transform fits for the arsenite and arsenate model compounds gave generally good fits over the edge (white line peak), but diverged in the region above the edge (Table 2). The model compounds (primary and secondary standards) thus may not be specifically present in the unknown spectra, but the strength and position of the white line for a given oxidation state (especially As^{3+} and As^{5+}) are characteristic within the unknown spectra. Transformed spectra for lower-oxidation-state standards and orpiment were found to be noisier than for the arsenate and arsenite transforms. This may be due to the lower abundance (or absence of) low-oxidation-state species in the spectra for the unknown species.

On the basis of the PCA (Table 2), model compounds were selected for linear combination XANES analysis of unknown spectra. We selected scorodite to represent As^{5+} species, arsenolite and schneiderhöhnite to represent As^{3+} species, and arsenopyrite and realgar to represent lower-oxidation-state compounds. The selected model spectra were initially applied in iterative trials, using different combinations of the above model spectra. All spectra were constrained to ±0.4 eV energy shifts during the fits. Schneiderhöhnite and arsenolite gave slightly different but reasonable fits as As^{3+} models. Where a lower-oxidation-state compound was required to improve the fit, both realgar (edge at 11,868 eV) and arsenopyrite (edge at 11,867 eV) gave reasonable results. These trials indicated that there is no overall improvement in the fits where schneiderhöhnite and realgar are used instead of arsenolite and arsenopyrite, even though the former compounds exhibit lower residuals in the PCA transform fits (Table 2). For consistency, arsenopyrite (As^{1-}) was chosen as the low-oxidation-state model compound in subsequent analyses, on the basis of the presence of relict arsenopyrite and As-rich pyrite in the tailings. Similarly, arsenolite was chosen as the As^{3+} model compound in preference to schneiderhöhnite, since it is a major by-product of the roasting process.

Electron-probe micro-analysis (EPMA)

Electron-probe micro-analysis was used to quantify total arsenic content in individual grains of roaster iron oxide. Analytical conditions for EPMA comprise an accelerating voltage of 15 kV, a take-off angle of 52.5°, an emission current of 100 mA, a beam current of *ca.* 40 nA, and analysis using energy-dispersion mode. Primary analytical standards for EPMA included scorodite from Laurium, Greece, for As, alunite from Marysville, Utah (Stoffregen & Alpers 1987) for S, kaersutitic amphibole for Na (Smithsonian USNM 143965) and a synthetic

glass for Fe, Al, Mg, Ca, and Si (US National Bureau of Standards 470). Synthetic magnetite and arsenolite were used as secondary standards to ensure accurate determination of Fe and As.

TABLE 2. SELECTION OF MODEL COMPOUNDS FOR LINEAR-COMBINATION-FIT XANES ANALYSIS

Standard	Formal state of oxidation of As	Residual of transform fit in PCA*	Quality of transform fit**		Selected for linear-combination-fit XANES analysis
			At the edge	Above the edge	
Scorodite	+5	3.2	1	2	Yes
Na arsenate	+5	8.0	1	3	No
Arsenolite	+3	5.7	1	2	Yes
Schneiderhöhnite	+3	3.9	1	2	Yes
Na arsenite	+3	5.1	2	2	No
Orpiment	+3	9.7	3	2	No
Realgar	+2	4.6	2	2	Yes
Elemental As	0	6.1	2	3	No
Arsenopyrite	-1	5.4	2	2	Yes

* Residual as % under PCA target-transformation routine in WinXAS™.
** Visual assessment of transform fit: 1: little to no deviation, 2: deviation, 3: poor fit.
Standards in bold are model compounds used in linear-combination-fit results presented in this paper.

RESULTS

Petrography

The roaster calcine (M2M) contains predominantly silt-sized porous-textured iron oxides (maghemite and hematite) among fine sand and silt gangue (quartz, carbonates and silicates). The bulk texture of the calcine is grain-supported but poorly sorted, with a fine opaque matrix that probably comprises mostly submicrometric roaster iron oxides. The shoreline tailings sample (CB1bS3) is stratified fine sand comprising mostly quartz, carbonates and silicate gangue, with red-brown silt interbeds that contain numerous silt-sized roaster iron oxide grains.

Both the mill calcine and the shoreline tailings contain roaster-derived iron oxides with concentric and spongy textures (Fig. 4). Some concentric-textured iron oxides rim pyrite in both the mill calcine and the shoreline tailings. Similar rims surrounding relict arsenopyrite are rarely observed in the mill calcine. A pyrrhotite-like phase is also present at low abundance in the mill calcine as free grains, rims on pyrite, and porous cores surrounded by concentric iron oxide. Pyrrhotite is an uncommon component in ore from the Giant mine, but it is an expected intermediate product in the roasting of both pyrite and arsenopyrite (Arriagada & Osseo-Asare 1984, Dunn et al. 1995). Iron oxides

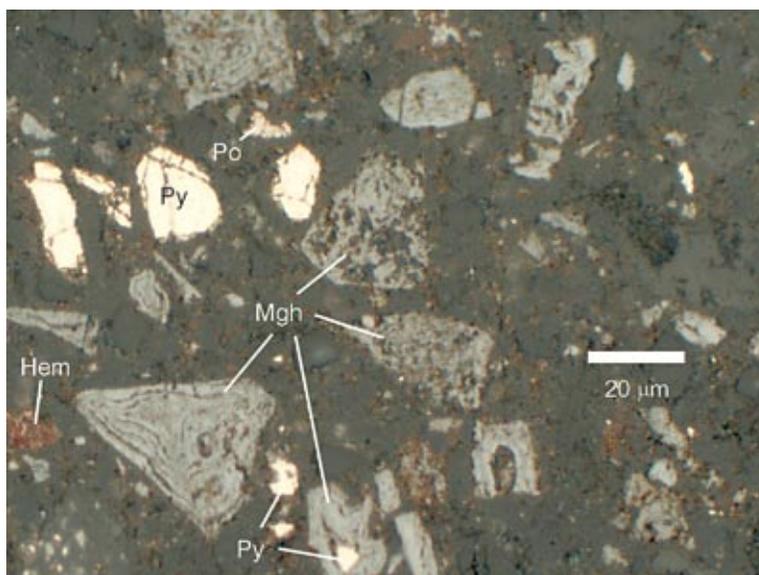FIG. 4. Reflected-light photomicrograph of calcine residue (roasted sulfide concentrate) from the Giant mine. Grey grains are arsenic-bearing roaster iron oxides that exhibit spongy and concentric textures. Roaster iron oxides are mostly maghemite (Mgh) with some hematite (Hem) that exhibits red internal reflections. Bright grains are relict sulfides, including yellowish white pyrite (Py) and brownish white pyrrhotite (Po).

in the mill calcine are also fragmented in some cases. This may be due to subsequent regrinding prior to cyanidation, or to explosive fracturing during roasting (Dunn *et al.* 1995). Some pyrite in the shoreline tailings also exhibits weathering as iron oxyhydroxide rims in both calcine-rich and calcine-poor zones. Under the optical microscope, very few roaster iron oxide grains exhibit bright red internal reflections characteristic of hematite, and even fewer exhibit a brownish hue more characteristic of magnetite.

Bulk XRD patterns

XRD patterns for the mill calcine (M2M) and the shoreline tailings (CB1bS3, calcine-rich and calcine-poor zones) are shown in Figure 5. Bulk XRD results have confirmed the presence of quartz, muscovite, chlorite and dolomite as the dominant crystalline phases in both the mill calcine and shoreline tailings, consistent with gangue mineralogy of the Giant ore

and petrographic observations. Minor phases including calcite, plagioclase and rutile have been identified by the presence of one or two major peaks. Maghemite (or magnetite) and pyrite are additional major components in the XRD pattern for the mill calcine (Fig. 5). Identification of maghemite instead of magnetite is based primarily on petrographic observations (see Discussion below). The broad peaks exhibited by maghemite are indicative of poor crystallinity. Hematite is not observed in the XRD trace of the mill calcine. However, the two strongest reflections for hematite (*d* values for 104 at 2.70 Å and 110 at 2.52 Å) may be obscured by the 200 peak of pyrite at 2.71 Å and the 311 peak of maghemite at 2.52 Å. Maghemite is also clearly identified in the calcine-rich portion of the shoreline tailings (Fig. 5).

Bulk XANES of mill calcine

The XANES spectrum for the bulk sample of mill calcine is shown in Figure 3. Mixed oxidation states

FIG. 5.   Bulk X-ray-diffraction results highlight the key interval for maghemite reflections (32 to 75° 2θ). Selected peaks for major phases (gangue) in this interval are labeled in the scan of the calcine-poor shoreline tailings (bottom, CB1bS3 calcine-poor). Pyrite and maghemite peaks are labeled in the scan of the mill calcine (top, M2M mill calcine). Maghemite is only weakly detected in the calcine-rich shoreline tailings (middle, CB1bS3 calcine-rich) and not detected in the calcine-poor sample, as expected. Scans are displaced vertically for purposes of presentation. The major peaks for quartz, chlorite and muscovite all occur at lower 2θ angles than the interval shown.

of arsenic, including As^{1-}, As^{3+} and As^{5+}, are identified, with contents of 9, 32 and 59%, respectively, by linear-combination fits of the reference spectra. The As^{1-} detected by XANES can be attributed to relict As-rich pyrite and arsenopyrite in the calcine, on the basis of their identification by petrography and bulk XRD. However, As^{3+} and As^{5+} cannot be attributed to a specific phase or phases.

EPMA data

No evidence of a distinct arsenic-rich phase was found in high-resolution back-scattered electron images of either the spongy or the concentric-textured iron oxides. Targets for point analyses were chosen to include both thick, concentric layers and "webs" within spongy grains. The arsenic content of the roaster iron oxide grains established by EPMA ranges from <0.5 to 7.6 wt.% As (Table 3), with the highest concentrations of As in the recent mill calcine. Grain-specific analytical results are presented in conjunction with μXANES and μXRD results, which follow.

μXANES and μXRD of roaster iron oxide grains

As in the case of bulk XANES, arsenic in mixed oxidation states is also detected within individual grain analyses of roaster iron oxides (Fig. 3). Linear-combination best-fit XANES results for the spectra in Figure 3 (Table 4) generally show little As^{1-} (<15%), and a greater amount of As^{3+} and As^{5+}. Pentavalent As is usually the dominant oxidation-state observed for most grains, but As^{3+} constitutes up to 52% of individual samples. Analysis of three opaque areas in the matrix of the mill calcine (e.g., Fig. 3, Table 4) confirms the same mixed oxidation-state (As^{3+} and As^{5+}) relationship, with typical concentrations of 40% As^{3+} and 60% As^{5+} and less than 5% As^{1-}. As previously noted, fitted model spectra at 5% or less gave little noticeable improvements to fits; values are included for consistency, however.

A further confirmation of the predominance of maghemite relative to magnetite is found in some μXRD patterns, which include a faint reflection (Debye–Scherrer ring) at 5.9 to 6.0 Å. Reference patterns of maghemite include a weak peak at approximately 5.9 Å, which is not present in magnetite.

A number of analytical results for discrete grains combining μXANES and μXRD are shown in Figures 6 to 8. Maghemite is, by far, the most common phase identified by μXRD of roaster iron oxide grains (e.g., Fig. 6) in both the calcine residue and shoreline tailings. Well-defined Debye–Scherrer powder patterns are observed for all μXRD images of roaster iron oxides (e.g., Figs. 6b, c), indicating that the average size of mineral crystallites is small relative to the diameter of the incident beam. As previously stated, individual crystallites at the beam scale under monochromatic X-rays would show up as discrete points or spotty rings, not the smooth rings observed for these grains. Roaster iron oxide grains are therefore interpreted to be poly-crystalline nanoparticulate composite grains. This is also consistent with the broad peaks observed by bulk XRD for maghemite in the mill calcine (Fig. 5).

Analyses confirm that for M2M (calcine), only grains exhibiting a spongy texture and red internal reflections contain hematite. The low modal abundance of these particles in the thin sections has limited the number of analyses of hematite grains to two. These analyses indicate that these grains are a mixture of maghemite and hematite, not just hematite (Figs. 6, 7b). No discrete arsenic-bearing phases were identified by μXRD of roaster iron oxide grains, even in grains with in excess of 5% As (w/w) (Figs. 8a, c). A maghemite grain mixed with hematite has also been observed in a grain in the shoreline tailings without an obvious spongy texture or red internal reflections (Figs. 8b, d).

A close inspection of individual Debye–Scherrer rings for hematite (Figs. 6c, 8d) reveals that they vary in intensity, in contrast to the rings for maghemite (Figs. 6b, 8c), which seem smoother. This is qualita-

TABLE 3. RESULTS OF ELECTRON-PROBE MICRO-ANALYSES (EPMA)
FOR ARSENIC

	Calcine residue (M2M)	Shoreline tailings (CB1bS3)
# grains analyzed	27	15
# analyses *	63	32
Mean	2.9 wt.%	1.3 wt.%
Standard deviation	1.7	0.6
Maximum	7.6	2.9
Minimum	<0.5	<0.5

* Between one and four analyses per grain, depending on size.

TABLE 4. RESULTS OF LINEAR-COMBINATION XANES FITS
OF SPECTRA IN FIGURE 4

Standard	M2M CA3	M2M CA AX1	M2M CA1	M2M (Bulk)
Arsenopyrite (As^{1-})	4 %	5 %	14 %	9 %
Arsenolite (As^{3-})	27	37	52	32
Scorodite (As^{5+})	69	58	34	59
Total As (% w/w)*	1.3 to 1.6	n.a.	1.5 to 2.2	2.5**
Description	Porous maghemite	Submicrometric matrix	Concentric rim of maghemite on pyrite	Calcine powder on Kapton

* Total As by EPMA except as indicated. Range given as maximum and minimum of two or more compositions.
** Total arsenic in bulk calcine sample (M2M) (Walker & Jamieson 2002).
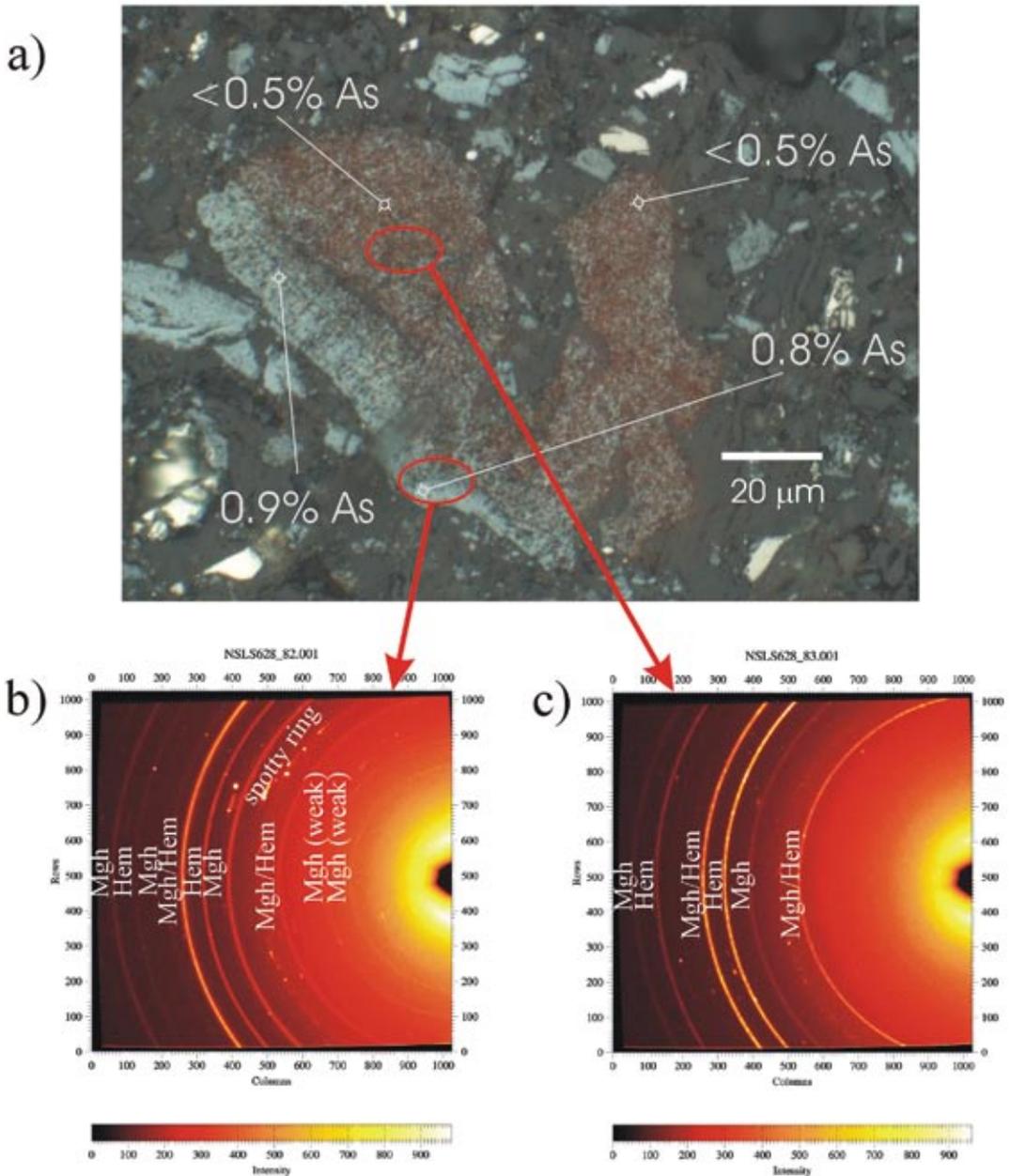n.a.: not available.

FIG. 6.   Micro-XRD results of a hematite-rich grain exhibiting red internal reflections. a) Photomicrograph of target grain with total arsenic established by EPMA indicated in white. Red ellipses indicate inferred footprint of the beam on sample selected for micro-XRD analyses. Micro-XRD patterns for two analyzed spots are shown below (b and c). Both XRD patterns show the presence of maghemite and hematite. More hematite occurs in the region exhibiting red internal reflections (c). The hematite rings in (c) are uneven in intensity, which suggests the presence of coarser crystallites of hematite. The spotty ring in (b) is probably due to reflections from fine gangue minerals, including chlorite, muscovite and quartz.

tive evidence of coarser crystallites of hematite than crystallites of maghemite, even where both minerals are present together within the same grain.

A mixture of As^{3+} and As^{5+} is consistently evident in maghemite grains with concentric and spongy textures, for both high and low arsenic content, with or without the presence of hematite, and for fresh calcine and 50-year-old subaerial (oxic) shoreline tailings. In the shore-
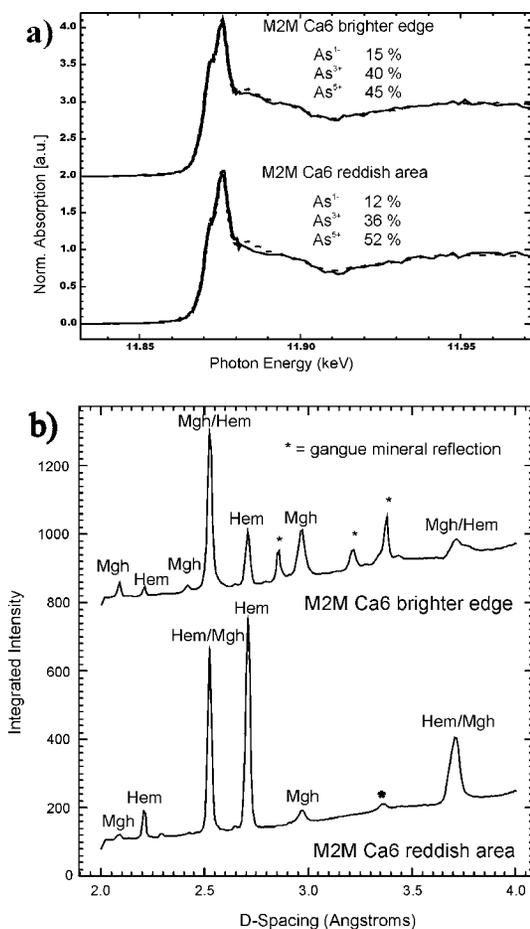

FIG. 7. Comparison of micro-XANES and micro-XRD for mixed hematite and maghemite grain in Figure 6. Only minor differences are evident in XANES results for maghemite-rich area (a, top) and hematite-rich area (a, bottom). Integrations of the micro-XRD patterns (Figs. 6b, c) clearly show that the bright edge is maghemite-rich (b, top), and the area with red internal reflections is mostly hematite (b, bottom). It should be noted that more maghemite is present in the analysis of the reddish area than would appear from the integrated pattern (b, bottom) owing to the overlap of the second strongest peak of hematite and the strongest peak of maghemite at 2.52 Å.

line tailings, this mixed oxidation-state relationship contrasts distinctly with arsenic associated with iron oxyhydroxides in the same thin section and even within grains located within 30 μm of each other (Fig. 9). The arsenic-bearing iron oxyhydroxide weathering-induced rims on pyrite show only As^{5+} with very little (if any) As^{3+}. The As^{1-} associated with iron oxyhydroxide grain in Figure 9 varies with the position of the beam on the grain (data not shown) and is consistent with As^{1-} associated with the pyrite core. Three XANES analyses for this grain yielded similar results to those in Figure 9 (As^{1-} from 13 to 24%), whereas in one scan, the As^{1-} determined amounts to 39%. For this latter sample, attempts to fit As^{3+} yielded negative concentrations, which is strong evidence that there is no As^{3+} in the iron oxyhydroxide rim of this grain.

DISCUSSION

Roaster iron oxides

As already discussed, roaster-derived iron oxides may consist of magnetite, maghemite or hematite. Magnetite and maghemite can be difficult to distinguish on the basis of XRD alone. Magnetite can be readily distinguished petrographically from hematite and maghemite on the basis of color in reflected light (brown-grey *versus* blue grey). The distinction between maghemite and magnetite in this study is based on petrographic observations rather than XRD alone.

The presence of maghemite in the roaster tailings from the Giant mine is not unexpected, considering that roasting was completed at 500°C in two stages, firstly at a low partial pressure of O_2, and secondly at a high partial pressure of O_2 (More & Pawson 1978). The maghemite probably formed by oxidation of a finely divided magnetite precursor (Cornell & Schwertmann 1996). Once formed, the maghemite is expected to transform to hematite between 370 and 600°C, depending on its origin and foreign ion content (Cornell & Schwertmann 1996, and references therein). We are not aware of specific studies on the thermal stability of arsenic-bearing maghemite; however, isomorphous substitution of aluminum for iron in maghemite (Wolska 1990) is known to increase its stability. The ionic radius of As^{3+} is between that of Fe^{3+} and Al^{3+}; structurally incorporated As may thus be possible and could increase the thermal stability of the maghemite. Further discussion concerning the speciation of arsenic in the roaster iron oxides is described below.

The low content of hematite in the Giant calcine is somewhat unexpected, since the second stage of roasting occurred with excess O_2, and roughly half of the sulfur as sulfide would have remained after the first stage of roasting (Jha & Kramer 1984). In the work by Eneroth & Koch (2003), significant quantities of nanocrystalline maghemite were formed during the thermal oxidation of pyrite at 500°C.

*The speciation of arsenic in roaster iron oxides
from the Giant mine*

Although nanocrystalline maghemite and hematite are clearly identified as hosts of the arsenic in the roaster iron oxides, there are a number of possible relationships between the arsenic and the iron oxides. Arsenic may be structurally incorporated into maghemite and hematite, surface-sorbed to high-surface-area maghemite and hematite, or present as finely dispersed crystalline or amorphous arsenic-bearing phase(s). The presence of both As^{3+} and As^{5+} adds another level of complexity to this relationship.

Only maghemite has been detected by μXRD in grains that have relatively high As content (*e.g.*, 5.6 wt.%, Figs. 8a, c), although up to 1.5 wt.% As has been detected in a grain containing both hematite and maghemite (Figs. 8b, d). The arsenic in these nanoparticle composite grains thus is not present as a separate crystalline phase or phases. However, the dual oxidation state observed by μXANES opens the possibility of finely dispersed nanocrystalline phase(s) at lower abundance than suggested by the total As measured by EPMA. For example, if we assume that all of the arsenic in Figure 8a (5.6 wt.%) is present as two nanocrystalline phases intergrown with maghemite, say scorodite (iron arsenate) and schneiderhöhnite (iron arsenite), the calculated modal amounts would be 17% and 4%, respectively. In such a case, we would expect detection of scorodite, but not necessarily schneiderhöhnite. Therefore, the possibility of separate finely dispersed nanocrystalline phase(s) cannot be completely eliminated. Crystalline iron arsenates seem unlikely, considering the above calculation. Soluble phases such as the As_2O_3 polymorphs arsenolite and claudetite also are unlikely, as they would be expected to dissolve in the calcine regrind-and-wash circuit or cyanide-leach circuit (More & Pawson 1978, Tait 1960).

Arsenate, a tetrahedral group, is not expected to enter the structure of hematite (McCreadie *et al.* 1998). The greater flexibility of the defect spinel structure makes some arsenate solid-solution in maghemite a possibility, but this has not been tested, and the high charge (5+) would need to be balanced. The similarity in ionic radius of As^{3+} to that of Fe^{3+} and Al^{3+} does suggest the potential for isomorphous substitution of arsenite in both hematite and maghemite. However, As^{3+} in arsenite minerals (*e.g.*, arsenolite, claudetite and schneiderhöhnite) exhibits trigonal pyramidal coordination with oxygen, whereas iron is in octahedral coordination in hematite, and octahedral or tetrahedral coordination in maghemite. Sites suitable for As^{3+} coordination may exist in the maghemite structure at defect sites, where an Fe^{3+} atom is missing as well as two or three of the coordinating oxygen atoms. The closest-packed nature of the oxygen atoms of the spinel structure presents an opportunity for trigonal pyramidal coordination of As^{3+} in such a defect.

It is possible that all of the As^{3+} and As^{5+} associated with these grains is strongly surface-sorbed as inner-sphere complexes, with the high concentrations of arsenic being further evidence of the nanocrystalline nature (high surface-area) of these grains. However, considering that these phases were formed at elevated temperature (approximately 500°C) in the presence of an arsenic-rich vapor, a structural association within the defect maghemite framework as well as a separate nanoscale X-ray-amorphous phase (*e.g.*, iron arsenate) or nanocrystalline phase (*e.g.*, iron arsenite) cannot be completely ruled out. The speciation of the lower-oxidation-state As (edge <11,868 eV) in the roaster iron oxides remains undetermined.

Investigating these roaster iron oxides in the context of their likely nanoparticulate nature is critical. In fact, recent synchrotron-excited photoelectron spectroscopy (SXPS) work by Schaufuss *et al.* (2000) on the oxidation of arsenopyrite at room temperature shows some striking similarities to our results, namely the presence of mixed oxidation-states at the surface of oxidizing arsenopyrite. At the Giant mine, the oxidation would have proceeded much more rapidly at elevated temperatures, and we observe the presence of weight percent concentrations of mixed oxidation-states of As on iron oxides derived not only from arsenopyrite, but also pyrite, which has concentrations of arsenic below one weight percent. However, the inferred high specific surface-area and nanoparticulate nature of these grains suggest that a comparison with the SXPS results is appropriate. This would not be the case if the roaster iron oxides had a macroscopic texture.

The total arsenic contents in iron oxides in the shoreline tailings are, on average, lower than those in the mill calcine (Table 3). Similarly, the lowest As^{3+} contents (on the order of only 10%) are also observed in the shoreline tailings (*e.g.*, Fig. 9). The roasting method differed at the time the shoreline tailings were deposited (Tait 1960), and it is not possible to determine whether the lower total arsenic and lower As^{3+} contents in the shoreline tailings are related to aging, leaching, processes of secondary mineralization, or the different conditions of roasting.

CONCLUSIONS

Arsenic speciation in roaster iron oxides

Roaster-derived iron oxides from the Giant mine contain up to 7 wt.% As. The arsenic in these grains is present in mixed oxidation-states, mostly as As^{3+} and As^{5+}. The arsenic concentrations and ratio of As^{3+} to As^{5+} seem to vary with mineral association and age of tailings, but additional work is necessary to better elucidate these relationships. The persistence of maghemite and As^{3+} in 50-year-old subaerial tailings suggests that these arsenic-bearing anthropogenic iron

oxides are stable during prolonged exposure in an oxic environment.

Maghemite is metastable with respect to hematite. However, as pointed out by Majzlan *et al.* (2003), the small difference in free energies between these phases can be altered by small changes in chemical composition (*e.g.*, Al substitution or, perhaps in this case, As), or physical properties such as grain size. Alternatively, kinetic barriers may inhibit crystal growth or transformations. The presence of either structural or surface-sorbed As is likely to increase resistance to such transformations (Cornell & Schwertmann 1996). The significant amount of As^{3+} remaining in the shoreline tailings roaster-iron oxides after 50 years of exposure contrasts with the As^{5+} association (*i.e.*, lack of As^{3+}) observed for weathering rims of iron oxyhydroxide on pyrite in the same material. The mixed oxidation-state of arsenic and the nanocrystalline nature of these iron oxides may have important implications when it comes to bio-availability and long-term stability, particularly under reducing conditions. Indirect evidence has been provided that other arsenic-bearing roaster-derived iron oxides are subject to microbially mediated reductive dissolution at the base of a tailings impoundment in northern Ontario (Stichbury *et al.* 2000).

Coincident μXRD and μXANES

Monochromatic μXRD using a two-dimensional CCD detector can be a powerful tool that quickly confirms in a qualitative manner the scale of crystallites within complex particles under the synchrotron beam. Specifically, i) amorphous phases or individual crystals at the beam scale result in no reflections (except in the unique case of a single crystal oriented such that it satisfies the Bragg condition), ii) fine crystallites at the micrometer scale result in spots, spotty rings and arcs, and iii) nanocrystalline phases result in well-defined smooth rings. In this study, the broad peaks for maghemite in the bulk XRD pattern of calcine suggest the existence of nanocrystalline maghemite. However, more dilute materials such as bulk tailings, sediments and soils will rarely contain sufficient phases of interest to assess the degree of crystallinity using bulk XRD. More importantly, μXRD is capable of confirming the presence of low-abundance crystalline phases (*e.g.*, hematite in this study) and the spatial relationship of multiple phases (*e.g.*, hematite and maghemite) that could not be determined by bulk XRD methods.

If linked with results from other synchrotron techniques, such as μXRF and μXANES, the coincident collection of information on chemical composition, mineralogy and oxidation state at a 10-μm spatial resolution can be very powerful. In this case, the mixed As^{3+} and As^{5+} states have been shown to be present for concentric and spongy maghemite, with or without the presence of hematite and for a range of arsenic content (<0.5 to 7 wt.% As). However, it is also apparent that for arsenic, low-oxidation-state species in low abundance relative to As^{3+} and As^{5+} are difficult to resolve, despite the difference in oxidation states. This is because the shift in edge position measured for a number of possible inorganic As–S compounds and elemental As by XANES is small (<2 eV), and they are at sufficiently low modal abundance that they are unlikely to be detected by μXRD.

The non-destructive nature of synchrotron radiation allows for subsequent analysis of the same targets by other microbeam techniques (such as EPMA in this case) or repeat analyses on the same grains at a later time. For arsenic and other redox-sensitive species, the ability to rapidly measure mineralogy by XRD (minutes) and oxidation state by XANES (tens of minutes) provides a means to measure or monitor alteration of sensitive phases due to microbeam influences (synchrotron or other techniques). As pointed out by Manceau *et al.* (2002), care must be exercised in preparing thin sections in order to eliminate or minimize the possibility of influences by the techniques of preparation on the speciation of solid phases. In this study, the results of bulk XANES analysis for calcine material confirm that the mixed oxidation-state of arsenic observed in individual grains is not a result of thin section preparation. In addition, such concerns are not limited to thin section preparation alone, but extend to all aspects of handling and techniques of preservation of solid samples. We believe that bulk and micro-analytical approaches similar to those described in this paper can be applied not only to the speciation and characterization of solids, but also to further the understanding of potential effects of sample handling on solid-phase speciation.
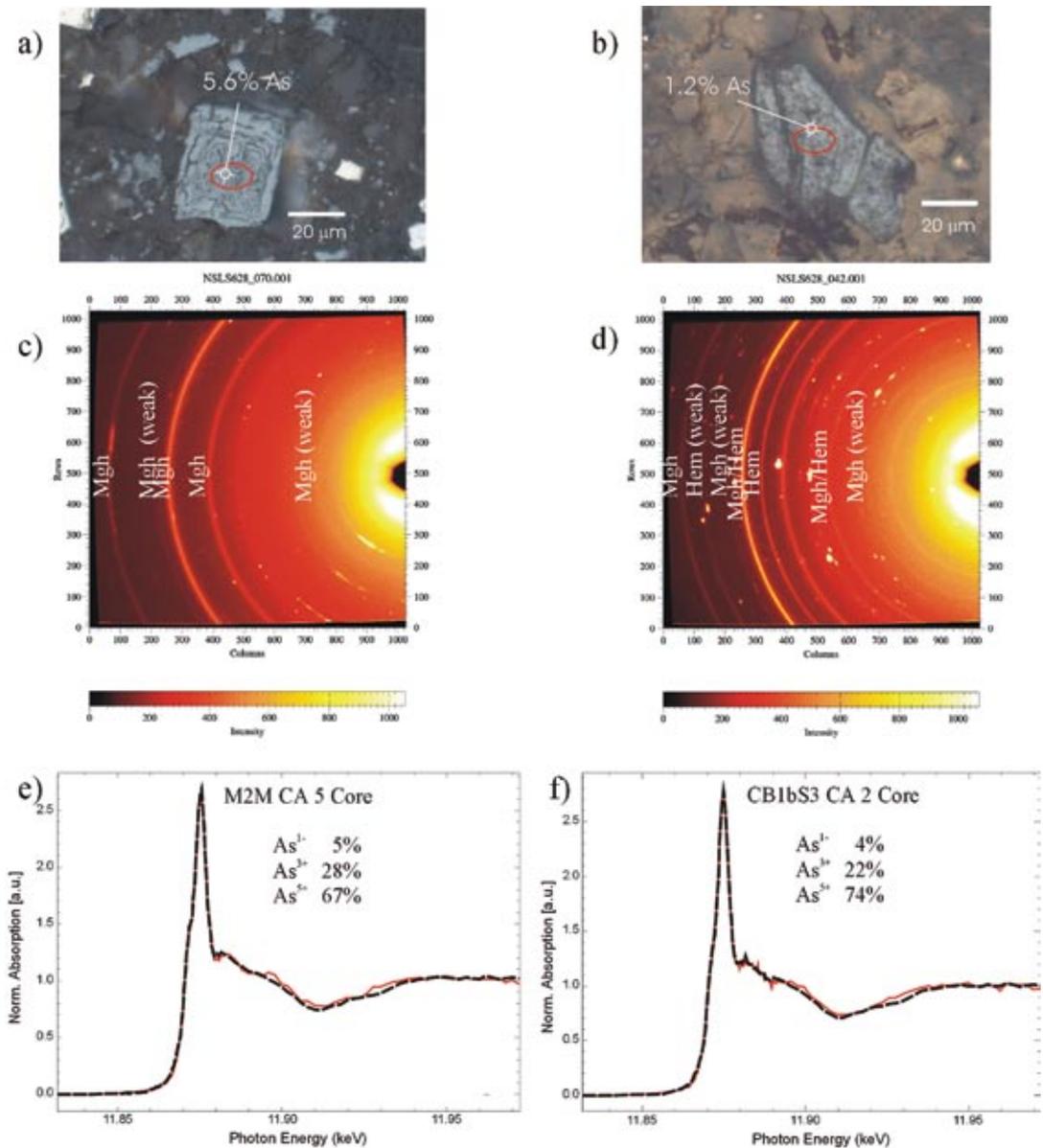
FIG. 8.   Selected analyses of two grains of roaster iron oxides. a) Reflected-light photomicrograph of square concentric roaster iron oxide from calcine sample (M2M). Total As established by EPMA (designated in white). b) Transmitted- and reflected-light photomicrograph of target grain from shoreline tailings sample (CB1bS3). Total As by EPMA as indicated. c) micro-XRD image of target in a) (red ellipse). Pattern is maghemite. Three arcs in lower right-hand corner are chlorite reflections. d) Micro-XRD image of target in b) (red ellipse). Pattern is a mixture of maghemite and hematite. e) Micro-XANES analysis of target in a) (red ellipse). Sample spectrum is in red, dashed line is best-fit linear combination for result shown. f) Micro-XANES analysis of target in b) (red ellipse).
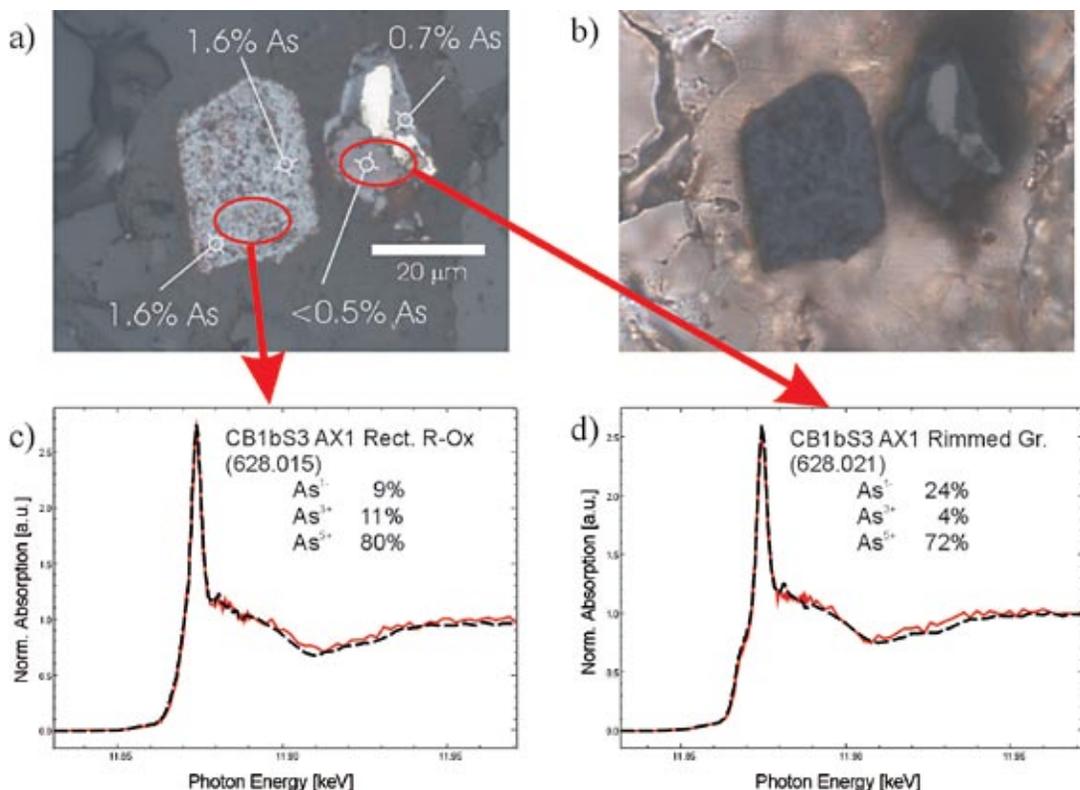
Fig. 9.   Comparison of oxidation state of As in shoreline tailings grains of various origins. a) Reflected-light photomicrograph of roaster iron oxide (left) and weathered pyrite with rim of iron oxyhydroxide (right). Target locations of XANES analyses are red ellipses, and those of EPMA analyses are indicated in white. b) Transmitted- and reflected-light photomicrograph of same area as in a), showing that a sizeable portion of the iron oxyhydroxide grain is buried in the section. c) Micro-XANES analysis of the roaster iron oxide. Dashed line is linear-combination best fit for results shown. Solid red line is XANES scan. d) Micro-XANES analysis of the iron oxyhydroxide rim. Of particular note in this case is that little or no As^{3+} is detected in the iron oxyhydroxide, in contrast to the roaster iron oxide.

REFERENCES

ARRIAGADA, F.J. & OSSEO-ASARE, K. (1984): Gold extraction from refractory ores: roasting behavior of pyrite and arsenopyrite. *In* Precious Metals: Mining, Extraction, and Processing (V. Kudryk, D.A. Corrigan & J. Liang, eds). TMS–AIME, New York, N.Y. (367-385).

BANFIELD, J.F. & ZHANG, H. (2001): Nanoparticles in the environment. *In* Nanoparticles and the Environment (J.F. Banfield & A. Navrotsky, eds.). *Rev. Mineral. Geochem.* **44**, 1-58.

BÉRUBÉ, Y., FRENETTE, M., GILBERT, R. & ANCTIL, C. (1973): Studies of mine waste containment at two mines near Yellowknife, N.W.T. *Indian Affairs and Northern Development Canada, Publ.* **QS–3038–000–EE–A1**, **ALUR 72–73–32**.

BHUMBLA, D.K. & KEEFER, R.F. (1994): Arsenic mobilization and bioavailability in soils. *In* Arsenic in the Environment. 1. Cycling and Characterization (J.O. Nriagu, ed.). John Wiley & Sons, Inc., New York, N.Y. (51-82).

BONAZZI, P., MENCHETTI, S., PRATESI, G., MUNIZ-MIRANDA, M. & SBRANA, G. (1996): Light-induced variations in realgar and β-As_4S_4: X-ray diffraction and Raman studies. *Am. Mineral.* **81**, 874-880.

BOSTICK, B.C. & FENDORF, S. (2003): Arsenite sorption on troillite (FeS) and pyrite (FeS_2). *Geochim. Cosmochim. Acta* **67**, 909-921.

BOYLE, R.W. (1960): The geology, geochemistry, and origin of the gold deposits of the Yellowknife district. *Geol. Surv. Can., Mem.* **310**.

CARTER, R. & SAMIS, C.S. (1952): The influence of roasting temperature upon gold extraction by cyanidation from

refractory gold ores. *Can. Inst. Mining Metall., Trans.* **55**, 120-126.

CORNELL, R.M. & SCHWERTMANN, U. (1996): *The Iron Oxides, Structure, Properties, Reactions Occurrences and Uses*. VCH, Weinheim, Germany.

CUMMINGS, D.E., CACCAVO, F., FENDORF, S. & ROSENZWEIG, R.F. (1999): Arsenic mobilization by the dissimilatory Fe(III)-reducing bacterium *Shewanella alga* BrY. *Environ. Sci. Technol.* **33**, 723-729.

DAVIS, A., RUBY, M.V., BLOOM, M., SCHOOF, R., FREEMAN, G. & BERGSTROM, P.D. (1996): Mineralogical constraints on the bioavailability of arsenic in smelter-impacted soils. *Environ. Sci. Technol.* **30**, 392-399.

DEB, P., BASUMALLICK, A., CHATTERJEE, P. & SENGUPTA, S.P. (2001): Preparation of α-Fe$_2$O$_3$ nanoparticles from a non-aqueous precursor medium. *Scripta Mater.* **45**, 341-346.

DUNN, J.G., GRAHAM, J. & NGUYEN, G.H. (1995): Textures of roasted pyritic concentrates and some modes of gold loss by cyanidation. *Aust. IMM Proc.* **1995**(1), 69-77.

DUTRIZAC, J.E. & JAMBOR, J.L. (2000): Jarosites and their application in hydrometallurgy. *In* Sulfate Minerals: Crystallography, Geochemistry, and Environmental Significance (C.N. Alpers, J.L. Jambor & D.K. Nordstrom, eds.). *Rev. Mineral. Geochem.* **40**, 405-452.

ELLIS, C.E. & HEARN, K. (1990): Operating mines. *In* Mineral Industry Report 1986–87 Northwest Territories (C.E. Ellis, ed.). NWT Geology Division, Department of Indian Affairs and Northern Development, Ottawa, Ontario (11-32).

ENEROTH, E. & KOCH, C.B. (2003): Crystallite size of haematite from the thermal oxidation of pyrite and marcasite effects of grain size and iron disulphide polymorph. *Minerals Eng.* **16**, 1257-1267.

ENG, P.J., RIVERS, M., YANG, B.X. & SCHILDKAMP, W. (1995): Micro-focusing 4 keV to 65 keV X-rays with bent Kirkpatrick–Baez mirrors. *In* X-Ray Microbeam Technology and Applications (W. Yun, ed.). *Proc. SPIE* **2516**, 41-51.

FENDORF, S.E. & SPARKS, D.L. (1996): X-ray absorption fine structure spectroscopy. *In* Methods of Soil Analysis. 3. Chemical Methods (J.M. Bartels, ed.). Soil Science Society of America, Inc. and American Society of Agronomy Inc., Madison, Wisconsin, USA (377-416).

FOSTER, A.L., BROWN, G.E., JR., TINGLE, T.N. & PARKS, G.A. (1998): Quantitative arsenic speciation in mine tailings using X-ray absorption spectroscopy. *Am. Mineral.* **83**, 553-568.

GOSSMAN, G.I. (1987): Pyrometallurgy of gold. *In* The Extractive Metallurgy of Gold in South Africa 1 (G.G. Stanley, ed.). *S. Afr. Inst. Mining Metall., Monogr.* **M7**, 345-377.

GREENWOOD, N.N. & EARNSHAW, A. (1998): *Chemistry of the Elements* (2nd ed.). Butterworth–Heineman, Oxford, U.K.

GRIMSEY, E.J. & AYLMORE, M.G. (1992): Mineralogical and chemical profile of a gold roaster. *Aust. IMM Proc.* **1992**(1), 43-49.

GROGAN, K.C. (1953): Treatment plant operation at Giant Yellowknife. *Can. Inst. Mining Metall., Trans.* **61**, 88-99.

HAMMERSLEY, A.P. (1998): FIT2D V10.3 Reference Manual V4.0. European Synchrotron Research Facility, Paper ESRF98–HA01T (program and manual available at http://www.esrf.fr/computing/expg/subgroups/data_analysis/FIT2D/).

HARVEY, C.F., SWARTZ, C.H., BADRUZZAMAN, A.B.M., KEON-BLUTE, N., YU, W., ALI, M.A., JAY, J., BECKIE, R., NIEDAN, V., BRABANDER, D., OATES, P.M., ASHFAQUE, K.N., ISLAM, S., HEMOND, H.F. & AHMED, M.F. (2002): Arsenic mobility and groundwater extraction in Bangladesh. *Science* **298**, 1602-1606.

HE, B.B. (2003): Introduction to two-dimensional X-ray diffraction. *Powder Diffraction* **18**, 71-85.

HENDERSON, P.J., MCMARTIN, I., HALL, G.E., PERCIVAL, J.B. & WALKER, D.A. (1998): The chemical and physical characteristics of heavy metals in humus and till in the vicinity of the base metal smelter at Flin Flon, Manitoba, Canada. *Env. Geol.* **34**(1), 39-58.

HERING, J.G. & KNEEBONE, P.E. (2002): Biogeochemical controls on arsenic occurrence and mobility in water supplies. *In* Environmental Chemistry of Arsenic (W.T. Frankenberger, Jr., ed.). Marcel Dekker, Inc., New York, N.Y. (155-181).

HOCHELLA, M.F., JR. (2002): There's plenty of room at the bottom: nanoscience in geochemistry. *Geochim. Cosmochim. Acta* **66**, 735-743.

HOCKING, D., KUCHAR, P., PLAMBECK, J.A. & SMITH, R.A. (1978): The impact of gold smelter emissions on vegetation and soils of a sub-arctic forest–tundra transition ecosystem. *J. Air Pollut. Control Assoc.* **28**(2), 133-137.

HUANG, P.M. & FUJII, R. (1996): Selenium and arsenic. *In* Methods of Soil Analysis. 3. Chemical Methods (J.M. Bartels, ed.). Soil Science Society of America, Inc. and American Society of Agronomy Inc., Madison, Wisconsin, USA (793-831).

ICDD (2003): Powder Diffraction File (PDF 2), Release 2003. International Centre for Diffraction Data, Newtown Square, Pennsylvania.

INSKEEP, W.P., MCDERMOTT, T.R. & FENDORF, S. (2002): Arsenic (V)/(III) cycling in soils and natural waters: chemical and microbiological processes. *In* Environmental Chemistry of Arsenic (W.T. Frankenberger, Jr., ed). Marcel Dekker, Inc., New York, N.Y. (183-215).

JAMBOR, J.L. (1994): Mineralogy of sulfide-rich tailings and their oxidation products. *In* Environmental Geochemistry of Sulfide Mine-Wastes (J.L. Jambor & D.W. Blowes, eds.). *Mineral. Assoc. Can., Short Course Vol.* **22**, 59-102.

_____ & BLOWES, D.W. (1998): Theory and applications of mineralogy in environmental studies of sulfide-bearing mine wastes. *In* Modern Approaches to Ore and Environmental Mineralogy (L.J. Cabri & D.J. Vaughan, eds.). *Mineral. Assoc. Can., Short Course Vol.* **27**, 367-401.

JHA, M.C. & KRAMER, M.J. (1984): Recovery of gold from arsenical ores. *In* Precious Metals: Mining, Extraction, and Processing (V. Kudryk, D.A. Corrigan & J. Liang, eds.). TMS–AIME, New York, N.Y. (337-365).

JORGENSEN, F.R.A. & MOYLE, F.J. (1981): Periodic thermal instability during the isothermal oxidation of pyrite. *Metall. Trans.* **12B**, 769-770.

MAJZLAN, J., GREVEL, K.-D. & NAVROTSKY, A. (2003): Thermodynamics of Fe oxides. II. Enthalpies of formation and relative stability of goethite (α-FeOOH), lepidocrocite (γ-FeOOH), and maghemite (γ-Fe$_2$O$_3$). *Am. Mineral.* **88**, 855-859.

MANCEAU, A., MARCUS, M.A. & TAMURA, N. (2002): Quantitative speciation of heavy metals in soils and sediments by synchrotron X-ray Techniques. *In* Applications of Synchrotron Radiation in Low-Temperature Geochemistry and Environmental Science (P.A. Fenter, M.L. Rivers, N.C. Sturchio & S.R. Sutton, eds.). *Rev. Mineral. Geochem.* **49**, 341-428.

MASSCHELEYN, P.H., DELAUNE, R.D. & PATRICK, W.H., JR. (1991): Effect of redox potential and pH on arsenic speciation and solubility in a contaminated soil. *Environ. Sci. Technol.* **25**, 1414-1419.

MCCREADIE, H., BLOWES, D.W., PTACEK, C.J. & JAMBOR, J.L. (2000): Influence of reduction reactions and solid-phase composition on porewater concentrations of arsenic. *Environ. Sci. Technol.* **34**, 3159-3166.

_____, JAMBOR, J.L., BLOWES, D.W., PTACEK, C. & HILLER, D. (1998): Geochemical behavior of autoclave-produced ferric arsenates: jarosite in a gold-mine tailings impoundment. *In* Waste Characterization and Treatment (W. Petruk, ed.). Society for Mining, Metallurgy, and Exploration, Inc., Littleton, Colorado (61-78).

MOK, W.-M. & WAI, C.M. (1990): Distribution and mobilization of arsenic and antimony species in the Coeur d'Alene River, Idaho. *Environ. Sci. Technol.* **24**, 102-108.

MOORE, J.N. & LUOMA, S.N. (1990): Hazardous wastes from large-scale metal extraction. *Environ. Sci. Technol.* **24**, 1278-1285.

MORE, M.A. & PAWSON, H.E. (1978): Giant Yellowknife Mines Limited. *In* Milling Practice in Canada (D.E. Pickett, ed.). *Can. Inst. Mining Metall., Spec. Vol.* **16**, 63-65.

MORIN, G., JUILLOT, F., CASIOT, C., BRUNEEL, O., PERSONNE, J.-C., ELBAZ-POULICHET, F., LEBLANC, M., ILDEFONSE, P. & CALAS, G. (2003): Bacterial formation of tooeleite and mixed arsenic(III) or arsenic(V)–iron(III) gels in the Carnoules acid mine drainage, France. A XANES, XRD, and SEM study. *Environ. Sci. Technol.* **37**, 1705-1712.

_____, LECOCQ, D., JUILLOT, F., CALAS, G., ILDEFONSE, P., BELIN, S., BRIOS, V., DILLMANN, P., CHEVALLIER, P., GAUTHIER, C., SOLE, A., PETIT, P.-E. & BORENSZTAJN, S. (2002): EXAFS evidence of sorbed arsenic(V) and pharmacosiderite in a soil overlying the Echassieres geochemical anomaly, Allier, France. *Bull. Soc. Géol. France* **173**, 281-291.

MORJAN, I., ALEXANDRESCU, R., SOARE, I., DUMITRACHE, F., SANDU, I. VOICU, I., CRUNTEANU, A., VASILE, E., CIUPINA, V. & MARTELLI, S. (2003): Nanoscale powders of different iron oxide phases prepared by continuous laser irradiation of iron pentacarbonyl-containing gas precursors. *Mater. Sci. Eng.* **C 23**, 211-216.

NAQVI, S.M., VAISHNAVI, C. & SINGH, H. (1994): Toxicity and metabolism of arsenic in vertebrates. *In* Arsenic in the Environment. II. Human Health and Ecosystem Effects (J.O. Nriagu, ed.). John Wiley and Sons, Inc., New York (55-91).

NAVROTSKY, A. (2001): Thermochemistry of nanomaterials. *In* Nanoparticles and the Environment (J.F. Banfield & A. Navrotsky, eds.). *Rev. Mineral. Geochem.* **44**, 73-103.

NICKSON, R.T., MCARTHUR, J.M., RAVENSCROFT, P., BURGESS, W.G. & AHMED, K.M. (2000): Mechanism of arsenic release to groundwater, Bangladesh and West Bengal. *Appl. Geochem.* **15**, 403-413.

PAKTUNC, D. & DUTRIZAC, J.E. (2003): Characterization of arsenate-for-sulfate substitution in synthetic jarosite using X-ray diffraction and X-ray absorption spectroscopy. *Can. Mineral.* **41**, 905-919.

_____, FOSTER, A., HEALD, S. & LAFLAMME, G. (2004): Speciation and characterization of arsenic in gold ores and cyanidation tailings using X-ray absorption spectroscopy. *Geochim. Cosmochim. Acta* **68**, 969-983.

_____, _____ & LAFLAMME, G. (2003): Speciation and characterization of arsenic in Ketza River mine tailings using X-ray absorption spectroscopy. *Environ. Sci. Technol.* **37**, 2067-2074.

RAGAINI, R.C., RALSTON, H.R. & ROBERTS, N. (1977): Environmental trace metal contamination in Kellogg, Idaho, near a lead smelting complex. *Environ. Sci. Technol.* **11**, 773-781.

REIMANN, C., BANKS, D. & DE CARITAT, P. (2000): Impacts of airborne contamination on regional soil and water quality: the Kola Peninsula, Russia. *Environ. Sci. Technol.* **34**, 2727-2732.

RESSLER, T., WONG, J., ROOS, J. & SMITH, I.L. (2000): Quantitative speciation of Mn-bearing particulates emitted from autos burning (methylcyclopentadienyl) manganese tricarbonyl-added gasolines using XANES spectroscopy. *Environ. Sci. Technol.* **34**, 950-958.

ROBINSON, J.J. (1988): The extraction of gold from sulphidic concentrates by roasting and cyanidation. *J. S. Afr. Inst. Mining Metall.* **88**(4), 117-130.

RUBY, M.V., SCHOOF, R., BRATTIN, W., GOLDADE, M., POST, G., HARNOIS, M., MOSBY, D.E., CASTEEL, S.W., BERTI, W., CARPENTER, M., EDWARDS, D., CRAGIN, D. & CHAPPELL, W. (1999): Advances in evaluating the oral bioavailability of inorganics in soil for use in human health risk assessment. *Environ. Sci. Technol.* **33**, 3697-3705.

SAVAGE, K.S., BIRD, D.K. & O'DAY, P.A. (2005): Arsenic speciation in synthetic jarosite. *Chem. Geol.* **215**, 473-498.

_____, TINGLE, T.N., O'DAY, P.A., WAYCHUNAS, G.A. & BIRD, D.K. (2000): Arsenic speciation in pyrite and secondary weathering phases, Mother Lode gold district, Tuolumne County, California. *Appl. Geochem.* **15**, 1219-1244.

SCHAUFUSS, A.G., NESBITT, H.W., SCAINI, M.J., HOECHST, H., BANCROFT, M.G. & SZARGAN, R. (2000): Reactivity of surface sites on fractured arsenopyrite (FeAsS) toward oxygen. *Am. Mineral.* **85**, 1754-1766.

SIMON, G., HUANG, H., PENNER-HAHN, J.E., KESLER, S.E. & KAO, L. (1999): Oxidation state of gold and arsenic in gold-bearing arsenian pyrite. *Am. Mineral.* **84**, 1071-1079.

SMEDLEY, P.L. & KINNIBURGH, D.G. (2002): A review of the source, behaviour and distribution of arsenic in natural waters. *Appl. Geochem.* **17**, 517-568.

SRK CONSULTING ENGINEERS AND SCIENTISTS (2002): Giant Mine, arsenic trioxide management alternatives, final report, December 2002. Prepared for Canadian Department of Indian Affairs & Northern Development, Yellowknife, NWT.

STICHBURY, M.-L.K., BAIN, J.G., BLOWES, D.W. & GOULD, W.D. (2000): Microbially-mediated dissolution of arsenic-bearing minerals in a gold mine tailings impoundment. *In* ICARD 2000, Proc. Fifth Int. Conf. Acid Rock Drainage **1**. Society for Mining, Metallurgy, and Exploration, Inc., Littleton, Colorado (97-103).

STOFFREGEN, R.E. & ALPERS, C.N. (1987): Woodhouseite and svanbergite in hydrothermal ore deposits: products of apatite destruction during advanced argillic alteration. *Can. Mineral.* **25**, 201-211.

STRAWN, D., DONER, H., ZAVARIN, M. & McHUGO, S. (2002): Microscale investigation into the geochemistry of arsenic, selenium, and iron in soil developed in pyritic shale materials. *Geoderma* **108**, 237-257.

TAIT, R.J.C. (1960): Recent progress in milling and gold extraction at Giant Yellowknife Gold Mines Limited. *Can. Inst. Mining Metall., Trans.* **64**, 204-216.

VALBERG, P.A., BECK, B.D., BOWERS, T.S., KEATING, J.L., BERGSTROM, P.D. & BOARDMAN, P.D. (1997): Issues in setting health-based cleanup levels for arsenic in soil. *Reg. Tox. Pharm.* **26**, 219-229.

WALKER, S.R. & JAMIESON, H.E. (2002): Mineralogical characterization of arsenic-bearing phases, Giant Mine Yellowknife Bay Tailings, Yellowknife, NWT. Unpublished report to Indian and Northern Affairs Canada, Yellowknife and Golder Associates Ltd., Vancouver, B.C.

WAYCHUNAS, G.A. (2001): Structure, aggregation and characterization of nanoparticles. *In* Nanoparticles and the Environment (J.F. Banfield & A. Navrotsky, eds.). *Rev. Mineral. Geochem.* **44**, 105-166.

WINSHIP, K.A. (1984): Toxicity of inorganic arsenic salts. *Adv. Drug React. Ac. Pois. Rev.* **3**, 129-160.

WOLSKA, E. (1990): Studies on the ordered and disordered aluminum substituted maghemites. *Solid State Ionics* **44**, 119-123.